Computational Methods to Accelerate Development of Corrosion Resistant Coatings for Industrial Gas Turbines

R. Pillai, K. Kane, M. Lance, and B. A. Pint

Abstract

Oxidation resistant overlay coatings protect the underlying superalloy component in industrial gas turbines from oxidation attack. Rate of depletion of the Al-rich β-phase in the bond coat governs the lifetime of these coatings. The applicability of a computational method in accelerating the development of corrosion resistant coatings and significantly reducing the extensive experimental effort to predict coating lifetimes and microstructural changes in three-coated Ni-based superalloys for real operational durations (20–40 kh) was undertaken in the present study. Scanning electron microscopy (SEM), energy dispersive X-ray spectroscopy (EDX), and electron microprobe analysis (EPMA) were employed to characterize MCrAlY-coated superalloy substrates (1483, 247 and X4) after exposure at 900 °C in air + 10% H_2O for up to 20,000 h. The model predicted the longest coating lifetime for the coating on X4 substrate. Precipitation of γ' in the coatings was correctly predicted for all three coating systems. Additionally, the model was able to predict the formation of topologically close packed (TCP)-phases in the investigated coating systems.

Introduction

Increasing the operating temperatures of gas turbines has become an increasingly common and effective strategy for improving engine efficiency and reducing fuel consumption. Protective metallic coatings enhance the oxidation and corrosion resistance of the underlying high temperature materials employed in industrial gas turbines. Some of the widely used types of coatings are MCrAlY (M = Ni, Co) overlay coatings and nickel aluminide (NiAl) diffusion coatings which ensure the growth of a slowly growing adherent alumina scale and thus protect the underlying substrate from rapid oxidation attack [1–3]. A suitable reservoir of Al (about 8–12 wt%) ensures formation of a protective alumina-based surface scale (thermally grown oxide, TGO) during high temperature exposure [4, 5]. MCrAlY coatings typically consist of γ-Ni and β-NiAl phases but may contain other complex phases such as σ-(Cr, Co), γ'-Ni$_3$Al, and/or α-Cr phases in substantial amounts depending on the coating composition and temperature [6–8]. Al from the coating material is lost to the external oxide layer on the surface and to the substrate by interdiffusion resulting in dissolution of the β-NiAl phase in the coating. Potentially detrimental precipitate phases may form especially in the interdiffusion zone (IDZ) during high temperature exposures which may significantly impact the integrity of the coating and the substrate and lead to unanticipated failures. Evaluation of the material's high temperature behavior and compatibility with a chosen coating requires extensive experimental testing, but computational methods can substantially reduce the extensive

R. Pillai (✉) · K. Kane · M. Lance · B. A. Pint
Materials Science and Technology Division, Oak Ridge National Laboratory, Oak Ridge, TN 37831-6156, USA
e-mail: pillairr@ornl.gov

experimental efforts required for coating evaluation and qualification.

In the current work, a coupled thermodynamic and kinetic computational model was employed to predict the microstructural evolution in overlay and nickel aluminide (NiAl) diffusion coatings on various Ni-based superalloys alloys during high temperature exposures in air. Similar modeling approaches have been successfully employed for multicomponent multiphase systems to describe the inter-diffusion in MCrAlY coating systems [9–13]. The wider applicability of the approach was further substantiated in understanding interdiffusion processes in multilayered coatings on Ni-based superalloys [8] and predicting the coating microstructure during over-aluminizing of an MCrAlY-coated Ni-based superalloy IN792 [14]. However, validation of these modeling methods with experimental observations has been reported for laboratory scale exposure times. Expected operational durations for gas turbines are of the order of 20–40 kh. In the present work, the results of the modeling procedure were compared with long-term labora-tory exposures for predicting:

1. lifetime of the coating in terms of the depletion of β-NiAl phase which usually leads to formation of undesirable oxides (due to critical depletion of Al)
2. formation of secondary phases in the coating, and
3. precipitation of potentially detrimental phases in the substrate.

Experimental Procedure

Investigated Materials

Substrate specimens (2 mm thick, ~ 16 mm diameter with chamfered edges) were grit blasted with alumina and then coated using a standard commercial-type, high velocity oxygen fuel (HVOF) process. The measured composition of the coating and substrates for all the investigated specimens is given in Table 1. In all cases, the coated substrates were annealed in a vacuum of 10^{-4} Pa (10^{-6} Torr) for 4 h at 1080 °C. All coatings were of the same NiCoCrAlY composition. Coatings were nominally 200 µm thick on X4 and about 180 µm thick on 247 and 1483 substrates.

High Temperature Exposures

Coated specimens were placed in alumina boats, heated to temperature to 900 °C for about 4 h in an alumina tube with flowing argon and then held for 500 h in flowing air with $10 \pm 1\%$ H_2O in a horizontal tube furnace. Carrier gas was typically flowed at 500 ml/min with distilled water atomized into the gas stream above its condensation temperature. Injected water was measured to calibrate its concentration. Mass change was measured every 500 h cycle using a Mettler–Toledo model XP205 balance.

Microstructural Characterization

After desired exposure time was reached, specimens were mounted in epoxy. The mounted samples were ground to 1200 grit with SiC grinding papers and subsequently pol-ished with diamond pastes to 0.5 µm surface finish. The final polishing step was made using colloidal SiO_2 slurry. Spec-imens were then examined by light microscopy. Electron probe microanalysis (EPMA) was performed using a JEOL model 8200 to obtain element concentrations and phase distributions. The scanning electron microscopy studies (SEM) were carried out using a TESCAN MIRA3 equipped with an energy dispersive X-ray (EDX) analysis system by EDAX Instruments. Phases were additionally identified by electron backscatter diffraction (EBSD).

Image analysis was performed with the open source software ImageJ [15] to measure the area fraction of the β-NiAl phase for comparison with model predictions. Color thresholding was employed on a selected region of interest 100×100 µm of optical microscopy images to differentiate between the observed phases in the coating. Area fractions were assumed to be equal to volume fractions. Additionally, oxide thicknesses and widths of each reaction zone (e.g., β-NiAl depletion zones, etc.) were measured from three loca-tions (20 measurements per location) using image analysis software ImageJ [15].

Table 1 Measured composition (inductively coupled plasma-optical emission spectroscopy) of the alloys in wt%

Alloy	Ni	Cr	Al	Co	Hf	Mo	Re	Ta	Ti	W	Y	Zr	C
Coating	50.1	16.5	12.3	21.1	–	–	–	–	–	–	0.7	–	–
X4	60.83	6.4	5.8	9.47	0.08	0.59	2.9	6.49	0.96	6.39	–	<0.01	0.004
1483	60.59	12.03	3.36	8.75	–	1.89	–	5.19	3.97	4.1	–	–	0.075
247	Bal.	8	5.5	9	1.5	0.7	–	3	1	9.5	–	0.03	0.06

The specimens were further etched with a 50 ml HCl + 2 ml H_2O_2 mixture for 5–10 s to impart suitable color contrast between the γ, γ', and β-NiAl phases in the micrographs. The etched cross sections provided additional evidence to identify the presence or absence of these phases.

Modeling Procedure

Homogenization Model

The coupled thermodynamic–kinetic approach to modeling the simultaneously occurring oxidation, diffusion, and dissolution processes occurring in the substrate-coating system has been described in detail elsewhere [13]. To enable realistic computational times for simulation of exposure duration of about 40 kh, the modeling procedure was modified further to allow calculations to be run on parallel computing cores [16]. A brief summary of the procedure will be mentioned here.

The procedure begins with the discretization of the domain into a suitable number of volume elements or slices of width Δz^i, i being the slice number. The position of the boundaries of these slices is marked as z^j, where $j = i + 1$. The center of the slices is marked as l^i. Average mole fractions N_c^{i0} for each constituent c are assigned to each slice based on the initial composition of the system. Constant molar volume V_m is assumed across the entire specimen. Initial phase fractions f_φ, compositions, and chemical potentials μ_c^i in each slice are defined by equilibrium calculations based on local element concentrations, temperature, and pressure. This is followed by choosing a suitable time step Δt for calculating diffusion of elements with the modified flux equation of Larsson et al. [17] in the lattice-fixed frame of reference. Efficient equilibration of vacancies ($\Delta \mu v_A = 0$) was assumed. The flux of each constituent in a slice J_c^i is evaluated as follows,

$$J_c^i = -\frac{M_c^{i,\text{eff}}}{V_m(l^{i+1} - l^i)} \sqrt{N_c^{i+1} N_c^i} 2 \sinh\left(\frac{\mu_c^{i+1} - \mu_c^i}{2RT}\right) \quad (1)$$

where $M_c^{i,\text{eff}}$ is the effective mobility of constituent c in slice i, μ_c^i is the chemical potential of constituent c at location i, R is the universal gas constant, and T is the temperature. Various alternatives to evaluate the local effective kinetic properties such as mobilities are documented in [18]. In this work, the upper Wiener bounds or more generally termed the "Rule of Mixtures" has been used with the phase fraction $f^\emptyset$ $M_c^\emptyset$ and mobility for the individual phase $\emptyset$ as follows,

$$M_c^{i,\text{eff}} = \sum_{\emptyset=1}^{\emptyset} f^\emptyset M_c^\emptyset. \quad (2)$$

Diffusion was considered to occur only in the γ (disordered face centered cubic, FCC), γ' (ordered FCC), β-NiAl (ordered body centered cubic, BCC), and α-Cr (disordered BCC) phases. Overall, the phases γ-FCC, γ'-FCC, β-BCC, α-Cr, σ, and μ-phase were considered for the calculations. Thermodynamic and kinetic data were taken from the databases TCNi8 [19] and MobNi4 [20], respectively.

Numerical Parameters

A geometric mesh was generated with a finer mesh at the alloy surface (left boundary\coating surface) and at the coating\substrate interface. Cell size was gradually increased toward the specimen center (right boundary). The mesh was adapted at each time step to account for the oxidation-induced metal loss (Al) at the coating surface. The mesh adaption procedure was explained in an earlier work [13]. The assumption of symmetry at the center of the sample provided the second spatial boundary condition of zero flux for all elements. Although formation of mixed oxides on surface of MCrAlY coatings is usually observed, a significant portion of the oxide scale is alumina. An outward flux of Al was prescribed by fitting the measured oxidation kinetics (not shown here) assuming exclusive formation of an alumina scale, while the system was closed for all other elements at the coating surface. The measured compositions of the base alloy in the as-received state given in Table 1 were used as the initial composition at time $t = 0$. The model provided average element concentrations and phase fractions as a function of time and distance.

Results and Discussion

Coating Lifetime

Coating lifetime is usually evaluated in terms of depletion of β-NiAl phase [9, 16]. The alloy composition strongly influenced the rate of β-NiAl depletion as Fig. 1 shows. Significant depletion of β-NiAl was observed in the coating on 1483 and 247, while a significant fraction of β-NiAl is still retained in the coating on X4. The fact that the coating on X4 was thicker (about 20 μm) than on 1483 and hence consisted of a larger β-NiAl reservoir cannot solely account for the observed lesser depletion as compositional differences between the substrates play a larger role. This will be discussed later in the text.

The calculated evolution of the average β-NiAl fraction in the coating over time is shown in Fig. 2. The measured phase fractions (from image analyses) are plotted in the same figure for comparison. The calculated average fractions of β-NiAl in the coating agree well with experimental observations.
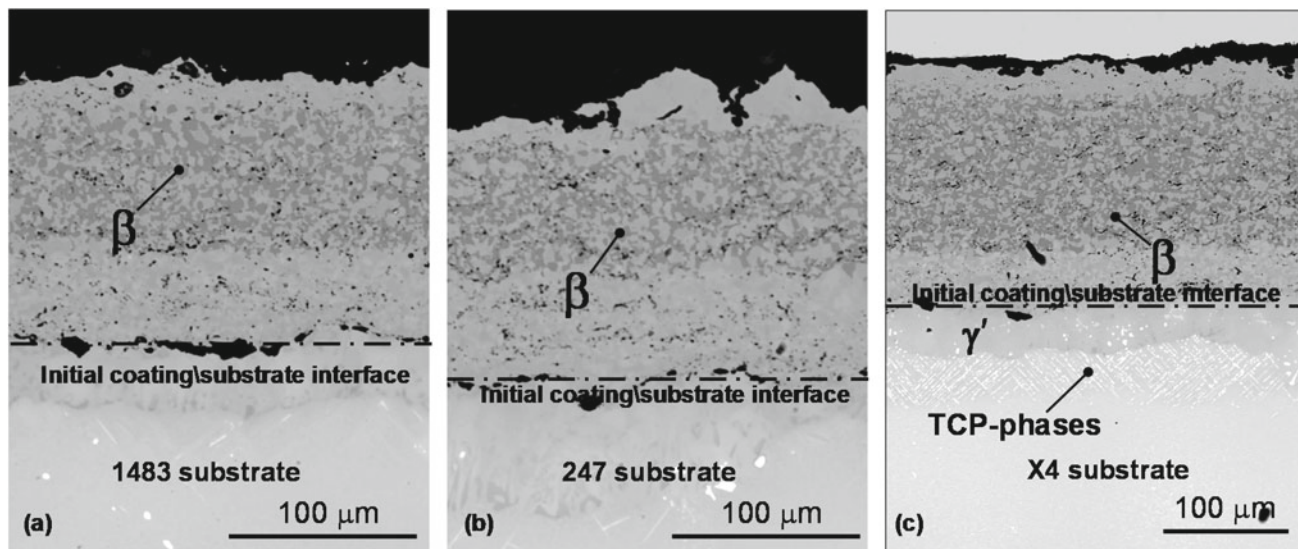
Fig. 1 Back scattered electron (BSE) images of metallographic cross sections of NiCoCrAlY coatings on the Ni-based superalloys **a** PWA1483, **b** 247, and **c** X4 after exposure in air + 10% H_2O for 20 cycles (10,000 h) at 900 °C [note the different scale bar on (**c**)]

Furthermore, the model correctly predicted that the coating on X4 will deplete much slower than on 1483. Coating on 1483 is predicted to completely deplete after about 21,500 h. Almost a complete depletion of β-NiAl was observed in the coating on 1483 after 20,000 h of exposure as is shown in Fig. 2. A coating lifetime of over 40,000 h was expected for X4. The reasons for this will be discussed now.

At 900 °C, coating depletion will mainly be governed by interdiffusion processes since the oxidation-induced depletion of Al is expected to be minimal. Interdiffusion processes between the coating and substrate are driven by gradients in chemical potentials (chemical activities) and diffusional velocities of alloying elements. Given the similar compositions of 1483 and 247, a detailed analysis will be given here for 1483 and X4 to demonstrate the role of alloy composition on coating lifetime.

The difference in the composition between 1483 and X4 reflects in the phase fractions of disordered γ-FCC and
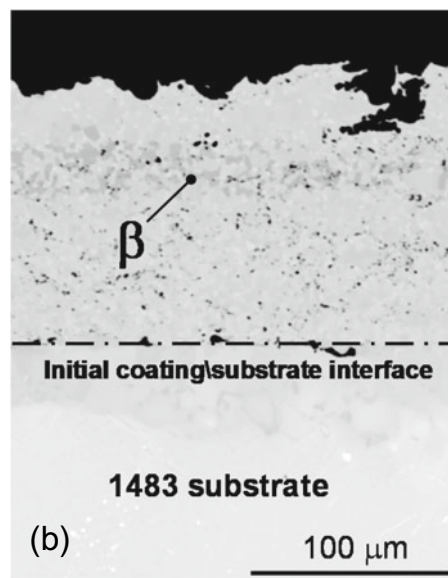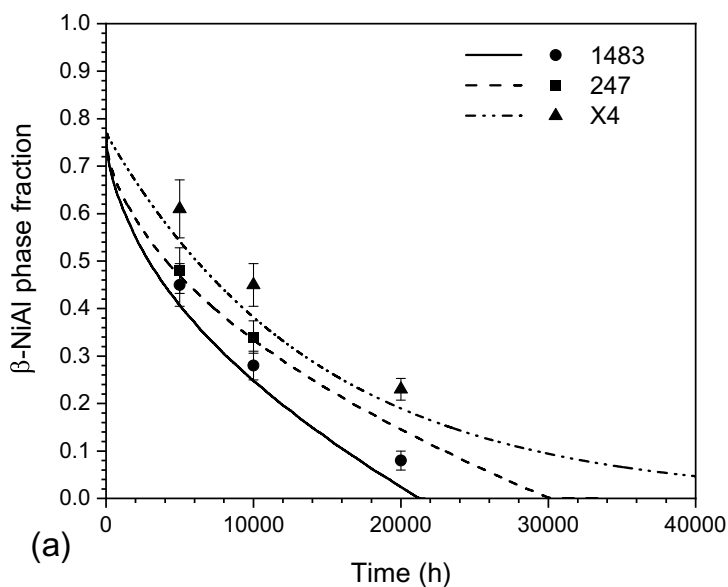
Fig. 2 **a** Calculated (lines) and measured (symbols, image analyses) average phase fraction of β-NiAl in the coatings on 1483, 247 and X4 substrates during exposure in air + 10% H_2O at 900 °C and **b** BSE image of cross section of NiCoCrAlY coating on 1483 after 40 cycles (20,000 h) in air + 10% H_2O at 900 °C. Dotted line indicates initial coating substrate interface
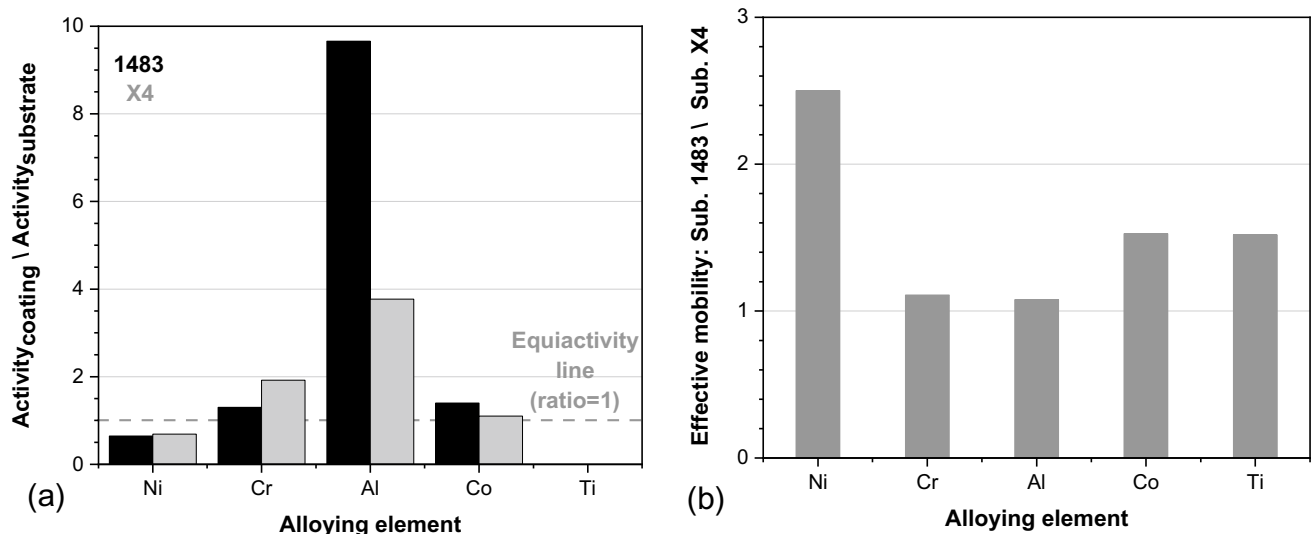
Fig. 3 Calculated ratio of **a** chemical activity in the coating to substrate (1483 and X4) and ratio of **b** effective mobilities of major alloying elements in 1483 to X4 at 900 °C for the compositions in as-coated state

ordered γ'-FCC. X4 consists of a much higher γ' phase fraction than 1483 (65 mol% compared to 45 mol% based on thermodynamic calculations) at 900 °C due to its higher Al and Ta content and the lower Cr content [21, 22]. Figure 3 shows the ratio of calculated chemical activities of major alloying elements Cr, Al, Ni, and Co in the coating to those in the 1483 and X4 substrates. A ratio greater than one means that the alloying element will diffuse from the coating to the substrate and from the substrate to the coating for ratios less than one. It is evident from the figure that the chemical activity gradient of Al is more than two times higher in case of 1483 than X4. In contrast, the driving force (gradient in chemical activities) for Cr to diffuse from the coating to the substrate is marginally higher in case of X4. The driving forces for diffusion of Co (coating to substrate) and Ni (substrate to coating) are almost identical for both substrates.

In addition to the chemical activity gradients, interdiffusion processes are further facilitated by diffusional velocities (mobilities in Eq. (2)) of alloying elements in the individual phases (mainly β-NiAl, γ, γ' in this case). Calculated mobilities of Ni, Cr, Al, and Co in the coating (γ–β) and substrate (γ–γ') at 900 °C are tabulated in Table 2.

It can be inferred from the table that the mobilities of Al and Ti in the γ-FCC phase are higher than those of Ni, Cr, and Co. However, the mobilities of Ni, Cr, and Ti in β-NiAl are almost 2–3 orders of magnitude higher than Co and Al. The mobilities of all elements in γ'-phase are 3–4 orders of magnitudes slower than in γ-FCC and β-NiAl.

Given these large differences in mobilities of Al in individual phases and combined with the highest gradient in chemical potentials for Al (Fig. 3), it is justified to assume that coating depletion will mainly be governed by interdiffusion of Al and Ni. The role of high Ti mobility in β-NiAl and hence in the coating strongly influences the phase transformations in the coating. This will be discussed in the next section. In addition to predicting the β-NiAl depletion in NiCoCrAlY coatings on the Ni-based superalloys X4, 247 and PWA1483 for exposure in air at 900 °C (500 h cycles), Table 3 shows that the measured and calculated widths of the β-NiAl depletion zones at the coating\substrate interface are in acceptable agreement.

Table 2 Calculated mobilities (mol m^2 J^{-1} s^{-1}) of major alloying elements in the coating (γ–β) and 1483 and X4 substrate phases (γ–γ') at 900 °C		Ni	Co	Cr	Al	Ti
Coating	γ-FCC	1.9e−8	9.3e−9	1.8e−8	5.9e−8	2.3e−8
	β-BCC	1.9e−6	6.6e−8	1.3e−6	1.1e−9	1.6e−6
1483	γ-FCC	2e−9	9.3e−9	7.6e−9	2.6e−8	2.5e−8
	γ'-FCC	6.3e−11	2.9e−9	3e−9	9e−9	5e−10
X4	γ-FCC	1e−9	6.2e−9	9e−9	3.3e−8	2.3e−8
	γ'-FCC	6.4e−11	2.5e−9	2.3e−9	6.7e−9	1.3e−10

Table 3 Comparison between the measured and calculated widths of the β–NiAl depletion zones at the coating\substrate interface

Alloy	Measured β–NiAl depletion zone (μm)/time (h)	Calculated β–NiAl depletion zone (μm)/time (h)	Predicted time to complete β–NiAl depletion (h)
X4	80 ± 10/20,000	100/20,000	>40,000
247	70 ± 5/10,000	65/10,000	30,000
1483	120 ± 10/20,000	140/20,000	21,500

The predicted time to complete depletion of β–NiAl phase is also shown

Microstructural Changes in the Coating

The presence of γ' was observed in the coating for all three coating systems at the coating\substrate interface. This is visible as a two-phase γ–γ' region in Fig. 4 showing the region at the coating\substrate interface for the three Ni-based superalloys after exposure in air + 10% H$_2$O at 900 °C for 10,000 h. This two-phase region is thinnest in case of the X4 substrate. Interestingly, etched metallographic cross sections and elemental maps indicate that γ' is also present at the interface between the β-NiAl depletion zone (oxide\coating interface) and the two-phase γ–β-NiAl coating. A similar effect has been reported to occur in overlay coatings on Ti, Ta-containing substrates [23].

Figure 5 shows the etched cross sections of the coating on 247 substrate at the oxide\coating (Fig. 5a) and coating \substrate (Fig. 5b) interfaces. Figure 6 shows the element distribution maps for Al and Ti at the phase interface in the coating, and it is evident that γ' is enriched at this location. The phases were further confirmed by measuring the phase compositions and were accordingly marked in Fig. 6. The calculated phase distribution (Fig. 7) after a 10,000 h exposure for the coating on 1483 correctly predicted the enrichment of γ' at the phase interfaces in the coating as observed in Fig. 5. The measured width of the zone with residual β-NiAl was 78 ± 6 μm compared to a calculated width of about 65 μm. The two-phase $\gamma + \gamma'$ region in the coating at the coating\substrate interface was measured to be 52 ± 5 μm which agrees well with the predicted value of 60 μm. A comparison between the measured (EDS) and calculated phase compositions is given in Table 4. Except

for a few deviations in the composition of the β-BCC phase which have been reported before [24, 25], the calculated phase compositions agree well with the measurements.

It is well known that Ti is a strong γ' stabilizer [26] and precipitation of γ' in the coatings investigated in the present work is mainly governed by the diffusion of Ti from the substrate to the coating. The combination of higher Ti content in 1483, relatively high mobility of Ti in β-NiAl (Table 2), relatively higher effective Ni mobility (Fig. 3) and diffusion of Al from the coating to the substrate supports formation of γ' in the coating. The reason for γ' enrichment at the phase interfaces mentioned above is most likely due to the significant differences in the mobilities of Al and Ti in individual phases. The mobility values in Table 2 suggest that at the interface between γ–β and γ–γ' phase regions, Ti would diffuse much faster away toward the interface into the γ–β region compared to Al into the γ–γ' substrate which would support formation of γ' at this interface.

Microstructural Changes in the Substrate

The interdiffusion processes resulted in enrichment of γ' in the substrate at the coating\substrate interface, typically observed after high temperature exposures of overlay NiCoCrAlY-type coatings [13, 27]. Furthermore, formation of TCP phases was observed in all three substrates after 10,000 h at 900 °C.

The predicted γ'-enrichment zone in the substrate was more pronounced in X4 comparison with 1483 and 247 (not shown here). As discussed before, X4 is expected to consist
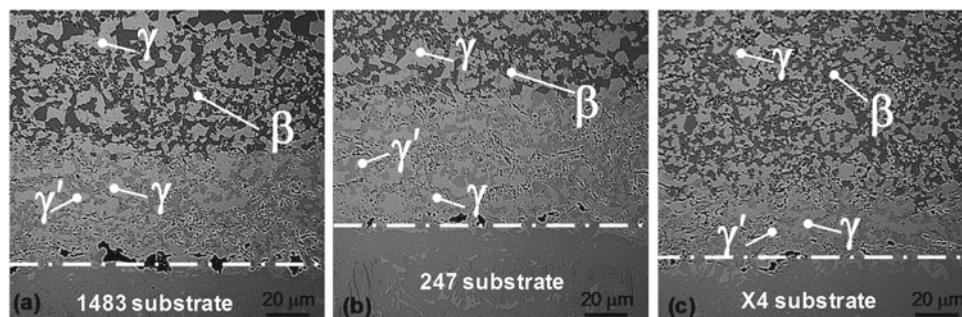
Fig. 4 BSE images of metallographic cross sections of NiCoCrAlY coatings on the Ni-based superalloys **a** PWA1483, **b** 247, and **c** X4 after exposure in air + 10% H$_2$O for 20 cycles (10,000 h) at 900 °C. Dotted line indicates initial coating substrate interface
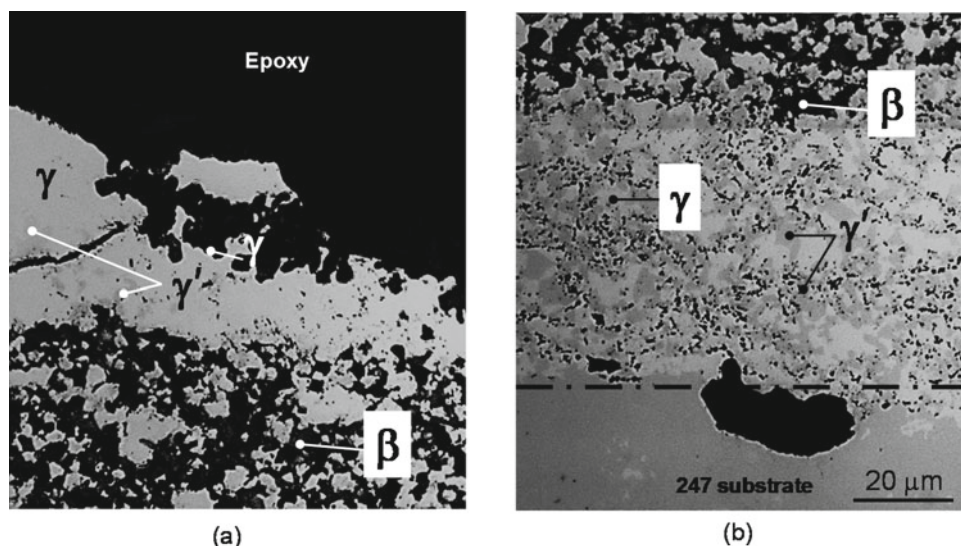
Fig. 5 Light microscopy images of etched cross sections of NiCoCrAlY coating on the Ni-based superalloy 247 at the **a** oxide\coating and **b** coating\substrate interface after exposure in air + 10% H₂O for 20 cycles (10,000 h) at 900 °C
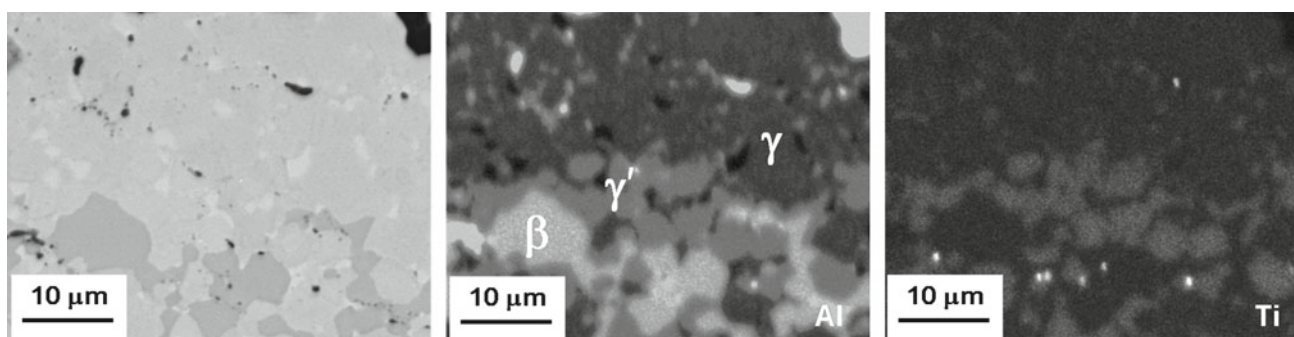
Fig. 6 Element distribution maps (EDS) of cross section of NiCoCrAlY coating on the Ni-based superalloy 1483 at the interface between the β–NiAl depletion zone (oxide\coating interface) and the two-phase γ–β–NiAl coating after exposure in air + 10% H₂O for 40 cycles (10,000 h) at 900 °C

of the highest fraction of γ′ among all alloys due to the higher Al and Ta contents. The diffusion of Al from the coating to the substrate during high temperature exposures further stabilizes γ′ at the coating\substrate interface.

Element distribution maps of major elements in the TCP phase observed in X4 indicate this phase to be rich in Cr, Re, and W (Fig. 8). The calculations predicted formation of a σ-phase in the X4 substrate. The reasoning for the formation of TCP phases in a NiCoCrAlY-coated X4 substrate has been provided in a previous work [13]. Diffusion of Al and Cr from the coating increases their activities at the coating substrate interface. The much lower mobilities of refractory elements such as Mo, Re and W result in an enrichment of these elements at the interface. This simultaneous increase of chemical activities of Al and Cr and Mo, Re, W concentrations results in the formation of TCP phases. The

correlation between Cr activity and precipitation of σ-phase has been reported before [28].

Interestingly, the model predicted formation of a μ-phase in the 1483 substrate after 10,000 h (Fig. 7) and 20,000 h of exposure. However, EBSD phase analyses results shown in Fig. 9 indicate the presence of both σ and μ-phases in the 1483 substrate. It must be mentioned though that an unequivocal identification of phases could not be ensured due to the extremely small size of these precipitates. An evaluation of the available thermodynamic data for TCP phases using the TCNI8 database does seem to partly support the notion that σ-phase would be the only TCP phase to precipitate in X4 under these conditions. Figure 10 shows the calculated ternary Ni-Cr-Re section of the Ni-Al-Cr-Co-Mo-Ta-Ti-W phase diagram at constant concentrations for Al, Co, Mo, Ta, Ti, and W corresponding to
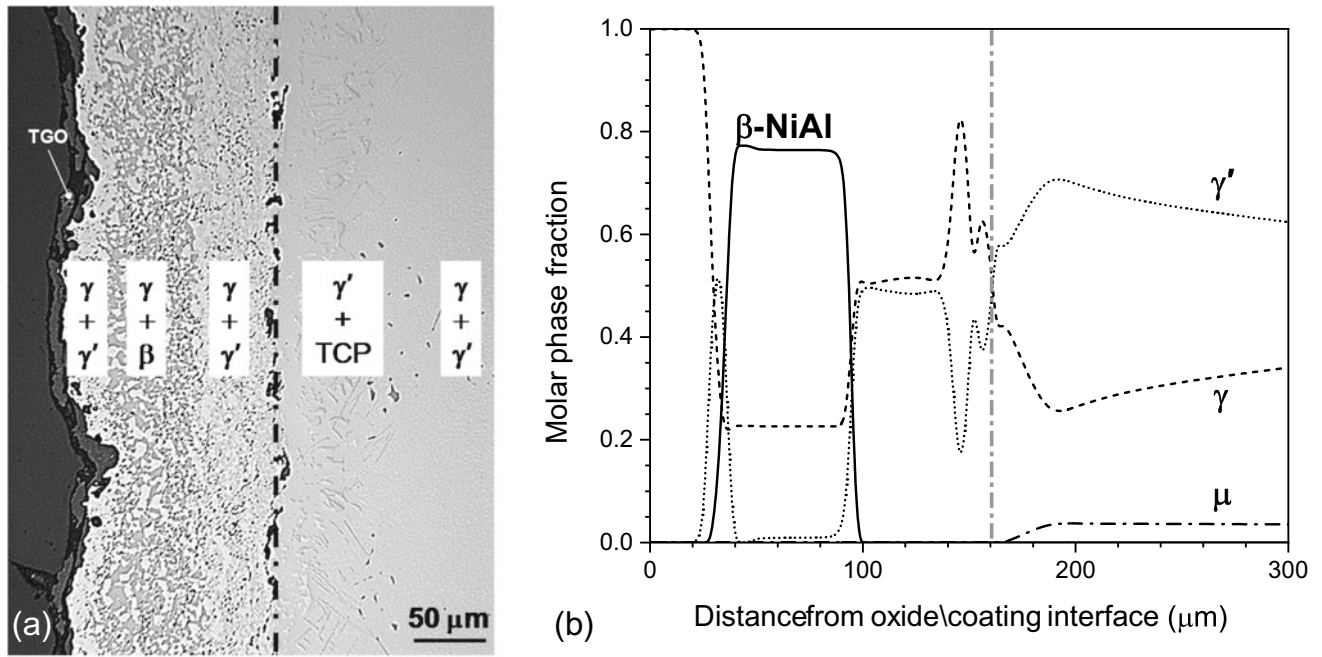
Fig. 7 **a** Back scattered electron (BSE) image of cross section of NiCoCrAlY coating on the Ni-based superalloy 1483 after exposure in air + 10% H_2O for 20 cycles (10,000 h) at 900° C (dotted line indicates initial coating substrate interface) and **b** corresponding calculated phase distribution

Table 4 Comparison between the measured and calculated phase compositions for the NiCoCrAlY coating on the Ni-based superalloy 1483 after exposure in air + 10% H_2O for 40 cycles (20,000 h) at 900 °C at the locations marked in Fig. 6

| Phase		Ni	Al	Ti	Cr	Co
β	Measured	47.97	34.46	0.22	4.51	8.28
	Calculated	43.92	27.71	0.43	11.41	16.74
γ'	Measured	57.24	18.25	1.37	7.09	11
	Calculated	61.23	19.27	2.81	4.78	11.72
γ	Measured	34.09	6.11	0.18	29.84	26.70
	Calculated	42.49	6.72	0.14	26.74	23.91
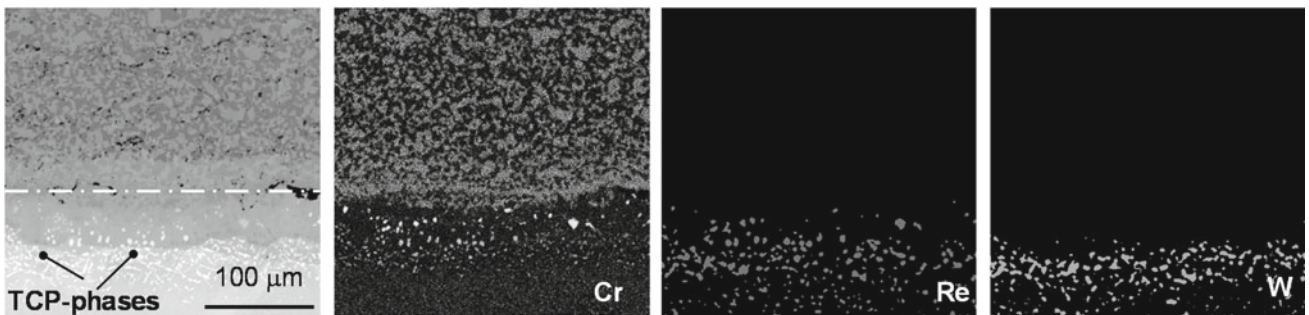
Fig. 8 Element distribution maps (EDS) for Cr, Re, and W of cross section of NiCoCrAlY coating on the Ni-based superalloy X4 after exposure in air + 10% H_2O for 20 cycles (10,000 h) at 900° C
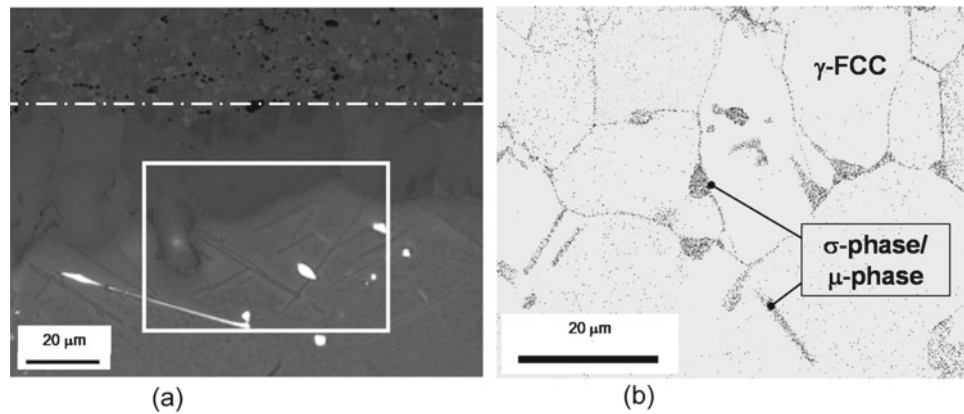
Fig. 9 **a** BSE image of cross section of NiCoCrAlY coating on the Ni-based superalloy 1483 at the coating\substrate interface (dotted line indicates initial interface) after 20 cycles (20,000 h) in air + 10% H$_2$O at 900 °C and **b** phases identified by EBSD in a selected region (box) of the BSE image for characterization of precipitates
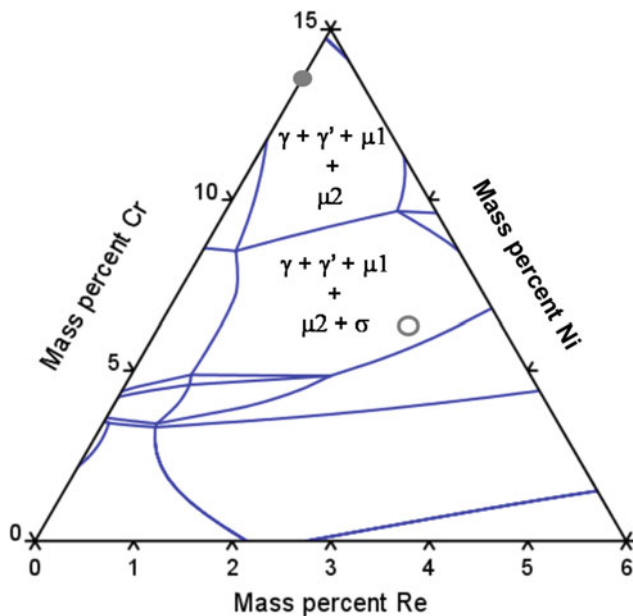
Fig. 10 Calculated ternary Ni-Cr-Re section of the Ni-Al-Cr-Co-Mo-Ta-Ti-W phase diagram at constant concentrations for Al, Co, Mo, Ta, Ti, and W corresponding to their average calculated values in the γ' enrichment zone on the substrate side at the coating \substrate interface after 40 cycles (20,000 h) in air + 10% H$_2$O at 900 °C

their average calculated values in the γ' enrichment zone on the substrate side at the coating\substrate interface after 20,000 h exposure at 900 °C. Although interdiffusion processes change the local concentrations for Cr and Re, this diagram aims to demonstrate solely the effect of Re on stability of TCP phases.

Solid symbol marks a non-Re containing 1483 composition, while the hollow symbol corresponds to X4 (with 2.9 wt% Re). Two different compositions of μ-phase are predicted in each case. Equilibrium calculations for 1483 (solid

symbol) indicate that only the μ-phase is expected to precipitate in 1483, but for X4 (hollow symbol), σ-phase will be the major TCP phase which seems to indicate that Re is stabilizing the σ-phase in X4. The calculated phase composition for the σ-phase was Cr34Co22W14Re12Ni18 at.%. The measured (EDS) composition of this phase was Cr43.8Co14.5W3.5Re4Ni27.3 at. %. The role of Re in stabilizing TCP phases in Ni-based superalloys has been investigated before [29, 30]. Since thermodynamic data for TCP phases is sparse and assessment of relevant data is based on high temperature data (>1000 °C), especially due to a lack of experimental data for temperature and composition dependent stability of these phases, a perfectly correct representation of the experimental observations and prediction of their stability should not be expected.

Summary and Conclusions

The computational approach helped understand the mechanisms of degradation of different oxidation resistant coatings on Ni-based superalloys. The highest lifetime was predicted for the coating on X4. Ti in the substrate material was expected to result in the formation of γ' in the coatings at the investigated temperature, and Re was expected to influence the type of precipitated TCP phases in the substrate as a result of interdiffusion processes. Such a strategy provides a general approach in predicting the coating lifetime, extent of microstructural changes in the coating and underlying substrate as a function of alloy/coating composition, time, and temperature. The validated model can greatly accelerate the design and selection of coatings for numerous superalloy applications.

References

1. Goward GW (1998) Progress in coatings for gas turbine airfoils. Surface & Coatings Technology 108(1–3) 73–79.

2. Quadakkers WJ, Shemet V, Sebold D, Anton R, Wessel E, Singheiser L (2005) Oxidation characteristics of a platinized MCrAlY bond coat for TBC systems during cyclic oxidation at 1000 degrees C. Surface & Coatings Technology 199(1) 77–82.

3. Haynes JA, Pint BA, Zhang Y, Wright IG (2007) Comparison of the cyclic oxidation behavior of beta-NiAl, beta-NiPtAl and gamma-gamma' NiPtAl coatings on various superalloys. Surface & Coatings Technology 202(4–7) 730–734.

4. Naumenko D, Shemet V, Singheiser L, Quadakkers WJ (2009) Failure mechanisms of thermal barrier coatings on MCrAlY-type bondcoats associated with the formation of the thermally grown oxide. Journal of Materials Science 44(7) 1687–1703.

5. Pint BA, Haynes JA, Zhang Y (2010) Effect of superalloy substrate and bond coating on TBC lifetime. Surface & Coatings Technology 205(5) 1236–1240.

6. Achar DRG, Munoz-Arroyo R, Singheiser L, Quadakkers WJ (2004) Modelling of phase equilibria in MCrAlY coating systems. Surface & Coatings Technology 187(2–3) 272–283.

7. Munoz-Arroyo R, Clemens D, Tietz F, Anton R, Quadakkers J, Singheiser L, Influence of composition and phase distribution on the oxidation behaviour of NiCoCrAlY alloys, in: R. Streiff, I.G. Wright, R.C. Krutenat, M. Caillet, A. Galerie (Eds.), High Temperature Corrosion and Protection of Materials 5, Pts 1 and 22001, pp. 165–172.

8. Pillai R, Taylor MP, Galiullin T, Chyrkin A, Wessel E, Evans H, Quadakkers WJ (2018) Predicting the microstructural evolution in a multi-layered corrosion resistant coating on a Ni-base superalloy. Materials at High Temperatures 35(1–3) 78–88.

9. Lee EY, Chartier DM, Biederman RR, Sisson RD (1987) Modeling the Microstructural Evolution and Degradation of MCrAlY Coatings During High-Temperature Oxidation. Surf. Coat. Tech. 32(1–4) 19–39.

10. Nijdam TJ, Sloof WG (2008) Modelling of composition and phase changes in multiphase alloys due to growth of an oxide layer. Acta Materialia 56(18) 4972–4983.

11. Karunaratne MSA, Di Martino I, Ogden SL, Oates DL, Thomson RC (2012) Modeling of Microstructural Evolution in an MCrAlY Overlay Coating on Different Superalloy Substrates. Metallurgical and Materials Transactions A 43(2) 774–788.

12. Yuan K, Eriksson R, Peng RL, Li X-H, Johansson S, Wang Y-D (2013) Modeling of microstructural evolution and lifetime prediction of MCrAlY coatings on nickel based superalloys during high temperature oxidation. Surface & Coatings Technology 232 204–215.

13. Pillai R, Sloof WG, Chyrkin A, Singheiser L, Quadakkers WJ (2015) A new computational approach for modelling the microstructural evolution and residual lifetime assessment of MCrAlY coatings. Materials at High Temperatures 32(1–2) 57–67.

14. Pillai R, Jalowicka A, Galiullin T, Naumenko D, Ernsberger M, Herzog R, Quadakkers WJ (2019) Simulating the effect of aluminizing on a CoNiCrAlY-coated Ni-base superalloy. Calphad-Computer Coupling of Phase Diagrams and Thermochemistry 65 340–345.

15. Schindelin J, Arganda-Carreras I, Frise E, Kaynig V, Longair M, Pietzsch T, Preibisch S, Rueden C, Saalfeld S, Schmid B, Tinevez J-Y, White DJ, Hartenstein V, Eliceiri K, Tomancak P, Cardona A (2012) Fiji: an open-source platform for biological-image analysis. Nature Methods 9(7) 676–682.

16. Chan KS, Cheruvu NS, Leverant GR (1998) Coating life prediction under cyclic oxidation conditions. Journal of Engineering for Gas Turbines and Power-Transactions of the Asme 120(3) 609–614.

17. Larsson H, Strandlund H, Hillert M (2006) Unified treatment of Kirkendall shift and migration of phase interfaces. Acta Materialia 54(4) 945–951.

18. Larsson H, Engstrom A (2006) A homogenization approach to diffusion simulations applied to alpha + gamma Fe-Cr-Ni diffusion couples. Acta Materialia 54(9) 2431–2439.

19. TCNi8, Thermo-Calc Software TCNi8/Ni-based superalloys database version 8, 2018.

20. MobNi4, Thermo-Calc Software MobNi4/Ni-alloys mobility database version 4, 2018.

21. Achar DRG, Munoz-Arroyo R, Singheiser L, Quadakkers WJ (2004) Modelling of phase distributions in MCrAlY coatings and their interactions with nickel based alloys. Journal De Physique Iv 120 231–238.

22. Chyrkin A, Swadzba R, Pillai R, Galiullin T, Wessel E, Gruner D, Quadakkers WJ (2018) Stability of External alpha-Al_2O_3 Scales on Alloy 602 CA at 1100–1200 A degrees C. Oxidation of Metals 90 (1–2) 119–133.

23. Naumenko D, Pillai R, Chyrkin A, Quadakkers WJ (2017) Overview on Recent Developments of Bondcoats for Plasma-Sprayed Thermal Barrier Coatings. Journal of Thermal Spray Technology 26(8) 1743–1757.

24. Gheno T, Liu XL, Lindwall G, Liu ZK, Gleeson B (2015) Experimental study and thermodynamic modeling of the Al-Co-Cr-Ni system. Sci Technol Adv Mat 16(5).

25. Liu XL, Gheno T, Lindahl BB, Lindwall G, Gleeson B, Liu ZK (2015) First-Principles Calculations, Experimental Study, and Thermodynamic Modeling of the Al-Co-Cr System. Plos One 10 (4).

26. Matthew J. Donachie SJD, Superalloys: A Technical Guide, 2 ed., ASM International 2002.

27. Pillai R, Wessel E, Nowak WJ, Naumenko D, Quadakkers WJ (2018) Predicting Effect of Base Alloy Composition on Oxidation- and Interdiffusion-Induced Degradation of an MCrAlY Coating. Jom 70(8) 1520–1526.

28. Anton R, Quadakkers J, Untersuchung zu den Versagensmechanismen von Wärmedämmschicht-Systemen im Temperaturbereich von 900°C bis 1050°C bei zyklischer Temperaturbelastung, RWTH Aachen, Julich, 2003.

29. Darolia R, Lahrman DF, Field RD (1988) Formation of topologically closed packed phases in Nickel base single crystal superalloys. Superalloys 1988 255–264.

30. Rae CMF, Karunaratne M, Small CJ, Broomfield RW, Jones CN (2000) Topologically close packed phases in an experimental Rhenium-containing single crystal superalloy. Superalloys 2000 767–776.